# **Extended Donnan-Manning Theory for Selective Ion Partition**

Revised Manuscript Submitted to Journal of Membrane Science as a Full-Length Article April 2023 Ruoyu Wang<sup>a</sup>, Ravindra Duddu<sup>a</sup>, and Shihong Lin\* a,b <sup>a</sup> Department of Civil and Environmental Engineering, Vanderbilt University, Nashville, Tennessee 37235-1831, USA <sup>b</sup> Department of Chemical and Bimolecular Engineering, Vanderbilt University, Nashville, Tennessee 37235-1831, USA \*Email: shihong.lin@vanderbilt.edu 

#### **Abstract**

22

23

24

25

26

27

28

29

30

31

32

33

34

35

36

The use of ion exchange membranes (IEMs) for electrochemical ion-ion separation leverages the selectivity of the IEMs toward like-charged species via valence difference and/or other ionmembrane interactions. A mechanistic model that relates selectivity with membrane structural and chemical properties is lacking in the literature. Here, we extend the Manning's counter-ion condensation model for describing ion partition and ion mobility inside IEMs to mixed salts scenarios. We evaluate the extended Donnan-Manning model against experimental data from literature and compare the performance the Donnan-Manning model to that of the ideal Donnan model and the Donnan-Affinity model. Our analysis shows that, despite its structural complexity, the Donnan-Manning model has less fitting parameters than the Donnan-Affinity model and generally outperforms the two other models in predicting counter-ion and co-ion partition. With the assumption of a higher mobility of condensed ions than that of uncondensed ions, the generalized Manning's model can also predict counter-ion mobility selectivity for cation exchange membranes, but its performance for predicting mobility selectivity for anion exchange membranes is still unsatisfactory.

37

38

40

39

**Keywords:** ion-ion selectivity, ion-exchange membrane, counter-ion condensation

#### 1. Introduction

Precise solute-solute separation is a topic of growing interest due to its relevance in resource extraction from brine lakes and seawater (e.g., lithium and rare earth elements extraction) and nutrient recovery from wastewaters (e.g., nitrogen and phosphorus recycling) [1–4]. Electrodialysis (ED) is one of the most promising membrane processes for selective ion-ion separation [5,6]. The key components that govern the performance of an ED process are ion exchange membranes (IEMs) which are dense polymer matrices with high density of fixed charge groups. IEMs allow the transport of counter-ions and repel co-ions and can thus achieve the separation of species with opposite charges. Historically, an ED process using alternately stacked cation exchange membranes (CEMs) and anion exchange membranes (AEMs) has been investigated most extensively for desalination [7–9]. However, recent studies have started to investigate ED for selective separations, hoping to leverage IEMs' selectivity between like-charged species based on valence difference and/or difference in ion-membrane affinity [10–14]. To guide the design of next generation IEMs for the specific application of ion-ion separation, fundamental understanding and quantitative description of selective ion transport through IEMs are critical.

Ion transport across the IEMs can be described by ion partition at two solution-membrane interfaces and ion transport inside the IEMs. Counter-ion selectivity of IEMs can be approximated by a product of partition selectivity at interfaces and mobility selectivity inside the membrane [5,15]. A desired IEM with high selectivity toward the ion of interest should prefer the partition and transport of target ion inside the membrane. To guide the design of IEMs with better selective separation ability, a mechanistic model that can relate selectivity with membrane structural and chemical properties is desired but still under development.

Ion partition to IEMs can be measured by static sorption experiments [16–18]. Donnan equilibrium is usually applied to predict the ion partition at solution-membrane interfaces but it only accounts for the ideal Donnan effect. Other models beyond the ideal Donnan model have been proposed to describe the ion partition. Donnan-Affinity model groups any non-ideal behavior during partition to an affinity term which results in a simple model with good fitting ability but lacks mechanistic insights on how to design better IEMs [11,19]. The Donnan-Manning model applies Manning's counter-ion condensation theory to describe ion transport across IEMs more

mechanistically but has only been validated with single salts [20–23]. However, ion transport with mixed salts can be very different from that with single salts and only mixed salts are practically relevant under the context of any selective separation [24].

Ion transport inside the IEMs can be described by the Nernst-Planck equations but requires the knowledge of accurate intra-membrane ion diffusivity. Ion diffusivity can be measured from salt diffusion experiments and membrane conductivity measurements for single salts or fitted from ED experiments with the prior measurement of ion partition for mixed salts [20,25]. Tortuosity effect is usually the only effect considered when modeling the diffusivity impediment inside IEMs [19]. Recently, models based on Manning's theory have been applied to account for the impeding electrostatic effect of fixed charges on ion diffusivity, but only for single salts [26,27]. Extension and validation of these models to mixed salts are necessary for the investigation of counter-ion selectivity of IEMs.

In this study, we first generalize the Manning's counter-ion condensation model to mixed salts. The generalized model is then validated with results from recent literature for di-/mono-valent and mono-/mono-valent ion partition experiments using both CEMs and AEMs. We also compare the generalized Donnan-Manning model with the ideal Donnan model and the Donnan-Affinity model on counter-ion selectivity and co-ion partition. We next discuss the impacts of membrane properties on counter-ion partition selectivity. Finally, we compare the model predictions of mobility selectivity to experimental results and discuss the possible reasons of the observed deviation.

#### 2. Theory

#### **2.1 Ion-ion selectivity**

The ion flux across the IEM,  $J_i$  [mol m<sup>-2</sup> s<sup>-1</sup>], can be modeled using the extended Nernst-Planck equations, considering advection flux, diffusion flux and electro-migration flux:

$$J_{i} = v_{w}c_{i}^{m} - D_{i}^{m}\frac{dc_{i}^{m}}{dx} - z_{i}c_{i}^{m}D_{i}^{m}\frac{F}{RT}\frac{d\varphi}{dx} \quad i = 1, 2, ...N_{s}$$
 (1)

where  $v_{\rm w}$  [m s<sup>-1</sup>] is the superficial water velocity across the membrane,  $D_i^{\rm m}$  [m<sup>2</sup> s<sup>-1</sup>] is the ion diffusion coefficient inside the membrane accounting for both tortuosity and porosity (i.e., water

volume fraction) effects,  $c_i^{\rm m}$  [mol m<sup>-3</sup>] is the  $i^{\rm th}$  ion concentration per volume of solution inside the IEM, x is the coordinate perpendicular to the membrane surface,  $z_i$  is the ion charge valence,  $\varphi$  [V] is the electrical potential, F [96487 C mol<sup>-1</sup>], R [8.314 J mol<sup>-1</sup> K<sup>-1</sup>] and T [K] are Faraday constant, ideal gas constant and absolute temperature, respectively.  $N_s$  is number of ion species. Ion-ion selectivity of a membrane process,  $S_{i/j}$ , is defined as the ratio of feed concentration-normalized ion fluxes between species i and j [5,15,24]. When electro-migration dominates the ion transport over diffusion and advection as in an ED process, the first two terms in Eq. (1) for ion flux can be ignored and the ion-ion selectivity can be approximated as the product of ion partition selectivity,  $S_{i/j}^R$ , and mobility selectivity,  $S_{i/j}^u$  [5,15]:

$$S_{i/j} = \frac{J_i/c_i^{s}}{J_i/c_i^{s}} \approx \left(\frac{K_i}{K_i}\right) \left(\frac{z_i D_i^{m}}{z_j D_i^{m}}\right) = S_{i/j}^{K} S_{i/j}^{u}$$
(2)

where  $c_i^s$  is the ion concentration of the (feed) solution phase concentration of i,  $K_i = c_i^{\rm m}/c_i^{\rm s}$  is the partition coefficient of ion i (same definitions apply for ion j). We note that the ion concentration ratio at the feed solution-membrane interface is used to evaluate  $K_i$ , as the main target is to selectively separate the ion of interest from the feed solution [5]. Partition selectivity,  $S_{i/j}^{K}$ , is defined as the ratio of partition coefficients. i.e.,  $K_i/K_j$ . Mobility selectivity,  $S_{i/j}^{u}$ , is defined as the ratio of ion mobility,  $u_i^{\rm m}/u_j^{\rm m}$  inside the IEM, where  $u_i^{\rm m} = z_i D_i^{\rm m} F/(RT)$  and  $u_j^{\rm m} = z_j D_j^{\rm m} F/(RT)$ .

## 2.2 Ion partition selectivity

#### 2.2.1 Ideal Donnan model

At ion sorption equilibrium, the electrochemical potential of ion *i* inside the IEM equals that in the external solution [28]:

$$\bar{\mu}_{i,0} + RT\ln(\gamma_i^{\mathrm{m}} c_i^{\mathrm{m}}) + z_i F \varphi^m = \bar{\mu}_{i,0} + RT\ln(\gamma_i^{\mathrm{s}} c_i^{\mathrm{s}}) + z_i F \varphi^{\mathrm{s}}$$
(3)

where  $\bar{\mu}_{i,0}$  [J mol<sup>-1</sup>] is the standard state chemical potential,  $\gamma_i^{\rm m}$  and  $\gamma_i^{\rm s}$  are activity coefficients of ion i in the membrane phase (i.e., inside the IEM) and the solution phase (i.e., outside the IEM),  $\varphi^{\rm m}$  [V] and  $\varphi^{\rm s}$  [V] are electrical potentials of the membrane phase and the solution phase. When assuming ideal solution behavior of ions for both phases (i.e.,  $\gamma_i^{\rm m} = \gamma_i^{\rm s} = 1$ ), Eq. (3) simplifies to:

$$c_i^{\rm m} = c_i^{\rm s} \exp\left(-\frac{z_i F}{RT} \Delta \varphi\right) \tag{4}$$

where  $\Delta \varphi = \varphi^{\rm m} - \varphi^{\rm s}$  is the Donnan potential across the solution-membrane interface and is same for every ion. Ion concentrations inside the IEM and the Donnan potential can be then solved using the local electro-neutrality condition:

$$\sum_{i} z_i c_i^{\mathrm{m}} + c_{\mathrm{x}} = 0 \tag{5}$$

where  $c_x$  [mol m<sup>-3</sup>] is the fixed charge density of the IEM per volume of absorbed solution (i.e., positive for AEMs and negative for CEMs) and is typically treated as spatially homogeneous. Thus, ion partition selectivity of the IEM with mixed salts can be expressed as:

$$S_{i/j}^{K} \equiv \frac{K_i}{K_j} = \frac{c_i^{\mathrm{m}}/c_i^{\mathrm{s}}}{c_j^{\mathrm{m}}/c_j^{\mathrm{s}}} = \exp\left(-\frac{\left(z_i - z_j\right)F}{RT}\Delta\varphi\right)$$
 (6)

Eq. (6) means the ideal Donnan model predicts ion partition selectivity as a function of ion valence difference and the Donnan potential which depends on the membrane charge density and the external solution composition. Eq. (6) suggests that  $S_{i/j}^K$  always equals one when ions i and j have the same valence, i.e., no selectivity is possible for ions with the same valence within the Donnan model framework.

## 2.2.2 Donnan-Affinity model

133

137

138

139

140

141

142

143

The Donnan-Affinity (D-A) model assumes that there is a difference between the chemical potential of the standard state of ions in the external solution ( $\bar{\mu}_{i,0}^{s}$ ) and that inside the IEM ( $\bar{\mu}_{i,0}^{m}$ ) [11,19]:

$$\bar{\mu}_{i,0}^{m} + RT \ln(c_i^{m}) + z_i F \varphi^{m} = \bar{\mu}_{i,0}^{s} + RT \ln(c_i^{s}) + z_i F \varphi^{s}$$
 (7)

This difference is quantified by  $\mu_i^{\rm ex} = \bar{\mu}_{i,0}^{\rm s} - \bar{\mu}_{i,0}^{\rm m}$ , where  $\mu_i^{\rm ex}$  [J mol<sup>-1</sup>] is the affinity (or excess chemical potential) of ion i due to all possible chemical and physical effects beyond the Donnan effect considered in the ideal Donnan model [11,19]. With this relatively flexible fitting parameter that broadly accounts for multiple effects, including solution non-ideality, the activity coefficients of ions are arbitrated to be unity to maintain model simplicity (one way to interpret this treatment is that the nonideal solution effects have been incorporated into  $\mu_i^{\rm ex}$ ). With these assumptions, the ion partition is given as:

$$c_i^{\rm m} = c_i^{\rm s} \exp\left(-\frac{z_i F}{RT} \Delta \varphi + \frac{\mu_i^{\rm ex}}{RT}\right) \tag{8}$$

The partition selectivity of the IEM with mixed salts can be then expressed as:

$$S_{i/j}^{K} = \exp\left(-\frac{(z_i - z_j)F}{RT}\Delta\varphi + \frac{\Delta\mu_{i/j}^{\text{ex}}}{RT}\right)$$
(9)

where  $\Delta \mu_{i/j}^{\rm ex} = \mu_i^{\rm ex} - \mu_j^{\rm ex}$  is the affinity (toward the IEM) difference between ions i and j. A positive  $\Delta \mu_{i/j}^{\rm ex}$  (i.e.,  $\mu_i^{\rm ex} > \mu_j^{\rm ex}$ ) means that ion species i is preferred over ion species j in partitioning into the IEM. We note that ion affinity is considered as an intrinsic property of the ion-IEM pair and is independent of concentration. Thus,  $S_{i/j}^K$  is a constant when ions i and j have the same valence, as the first term in the exponent of Eq. (9) equals zero and Eq. (9) is reduced to  $S_{i/j}^K = \exp(\Delta \mu_{i/j}^{\rm ex}/RT)$ . When using the D-A model, ion affinity terms are usually fitted from experimental sorption data, and theoretical estimation is currently unavailable [11,19].

## 2.2.3 Donnan-Manning model

153 Releasing the simplifying assumption of ideal solution behavior and without introducing an ion 154 affinity term as a fudge factor, Eq. (3) can be written as:

$$\gamma_i^{\rm m} c_i^{\rm m} = \gamma_i^{\rm s} c_i^{\rm s} \exp\left(-\frac{z_i F}{RT} \Delta \varphi\right) \tag{10}$$

where the ion activity coefficient for an ion in the solution phase,  $\gamma_i^s$ , can be estimated using the Pitzer model [29,30]. To estimate the ion activity coefficient inside the IEM, Manning's counterion condensation theory has been applied for a single salt system (i.e., the salt contains only one anion species and one cation species) [21,22]. Based on this theory, the IEM is modeled as a cross-linked network of linear polyelectrolyte chains with spatially even distribution of charges. When describing the local interaction between the fixed charges and ions, the Manning parameter (also known as dimensionless linear charge density) is defined as  $\xi = \lambda_{\rm B}/b$ , where  $\lambda_{\rm B} = e^2/(4\pi\varepsilon_0\varepsilon k_{\rm B}T)$  is the Bjerrum length and b is the distance between fixed charges [31,32]. The 'counter-ion condensation' in the Manning's theory refers to the phenomenon that part of counterions inside the IEM tend to stay in the overlapping electric fields of two adjacent fixed charges and behave differently from the free counter-ions, if  $\xi$  exceeds a critical value,  $\xi_{\rm cr} = 1/|z_x z_{\rm g}|$ , where  $z_x$  is membrane charge valence and  $z_{\rm g}$  is the counter-ion valence. In other words, counter-

ion condensation occurs when  $b < |z_x z_g| \lambda_B$ . From now on, we assume  $|z_x| = 1$  for simplicity (e.g., sulfonic acid groups in CEMs and quaternary amino groups in AEMs). The uncondensed ions are treated using Debye-Huckel approximation to account for point-to-line electrostatic forces.

170

171

172

173

174

175

182

183

184

185

Manning's counter-ion condensation theory has been successfully applied to describe single salts partition to IEMs [16,21,33–35]. However, the model has yet to be extended to describe mixed salts partition. The expressions for ion activity coefficients estimation are only derived for single salts and cannot be directly applied to mixed salts [20,32]. Herein, we extend the expressions for estimating ion activity coefficients inside IEMs based on Manning's theory [32,36] (see Appendix A1 for detailed derivation).

When no counter-ion condensation occurs (i.e.,  $\xi < \xi_{\rm cr}$ ),  $\gamma_i^{\rm m}$  of both counter-ions and coions can be estimated by:

$$\ln(\gamma_i^{\rm m}) = -\frac{\xi |c_{\rm x}| z_i^2}{2 \sum_i (z_i^2 c_i^{\rm m})}$$
(11)

Integrating Eq. (10) and (11), when no counter-ion condensation occurs, the partition selectivity can be then expressed as:

$$S_{i/j}^{K} = \frac{\gamma_i^s}{\gamma_j^s} \exp\left(-\frac{\left(z_i - z_j\right)F}{RT}\Delta\varphi - \frac{\xi |c_x|\left(z_j^2 - z_i^2\right)}{2\sum_i (z_i^2 c_i^m)}\right)$$
(12)

180 When counter-ion condensation occurs (i.e.,  $\xi > \xi_{\rm cr}$ ), co-ion and counter-ion activity coefficients 181 are given as:

$$\ln(\gamma_c^{\rm m}) = -\frac{\xi_{\rm cr}^2 |c_{\rm x}| z_c^2}{2\xi \sum_i (z_i^2 c_i^{\rm m} f_{{\rm u},i})}$$
(13)

$$\ln(\gamma_{g,i}^{m}) = \ln(f_{u,i}) - \frac{\xi_{cr}^{2} |c_{x}| z_{i}^{2}}{2\xi \sum_{i} (z_{i}^{2} c_{i}^{m} f_{u,i})}$$
(14)

where  $f_{u,i}$  is the fraction of counter-ion *i* inside the IEM that is in the uncondensed state. Consider a ternary case (i.e., two counter-ions and one co-ion for an IEM) and assume the partial condensation of both counter-ions [36], the uncondensed fraction of each counter-ion can be estimated by solving Eqs. (15-16) simultaneously:

$$|z_{i}|c_{i}^{m}(1-f_{u,i})+|z_{j}|c_{j}^{m}(1-f_{u,j})=|c_{x}|\left(1-\frac{\xi_{cr}}{\xi}\right)$$
(15)

$$\frac{\left|z_{j}\right|\left(1-f_{\mathrm{u},j}\right)/f_{\mathrm{u},j}}{\left|z_{i}\right|\left(1-f_{\mathrm{u},i}\right)/f_{\mathrm{u},i}} = \exp\left(\frac{\Delta\mu_{i/j}^{\mathrm{con}}}{RT}\right) \tag{16}$$

where Eq. (15) describes that condensed counter-ions screen a sufficient number of the fixed charges, Eq. (16) describes the counter-ion condensation equilibrium, and  $\Delta\mu_{i/j}^{\rm con}$  [J mol<sup>-1</sup>] is the condensation energy difference between the two counter-ions, similar to Manning's original treatment on the condensation equilibrium between two monovalent counter-ion species (c.f. Eq. (35) in reference [36]). Different from Manning's original assumption that the multi-valent counter-ions would condense prior to monovalent ions, we here assume both counter-ions may partially condense simultaneously when the Manning parameter is larger than the lowest critical value, i.e.,  $\xi > \min(\xi_{\rm cr,}i)$ . Moreover, to keep simplicity and reduce fitting parameters, we do not separately specify any finite volume effect of the condensed counter-ions as Manning did, but consider it has been accounted for in  $\Delta\mu_{i/j}^{\rm con}$ . Thus, the partition selectivity when counter-ion condensation occurs can be then expressed as:

$$S_{i/j}^{K} = \frac{\gamma_{i}^{s} f_{u,j}}{\gamma_{j}^{s} f_{u,i}} \exp\left(-\frac{(z_{i} - z_{j})F}{RT} \Delta \varphi - \frac{\xi_{cr}^{2} |c_{x}| (z_{j}^{2} - z_{i}^{2})}{2\xi \sum_{i} (z_{i}^{2} c_{i}^{m} f_{u,i})}\right)$$
(17)

We note that Eqs. (11, and 13–15) reduce to single salts scenario where the system contains only one counter-ion, i.e., when we have binary instead of ternary system (see Appendix A2 for derivation). The key step of generalization is to calculate the Debye screening parameter of the mixed electrolytes.

## 2.3 Mobility selectivity

Ion mobility inside IEMs is slower than that in the bulk solution due to both spatial and electrostatic effects [20,27]. The spatial effect considers the tortuosity of free volumes inside the IEM and is usually modeled by the Mackie-Mears model [37]. The electrostatic effect of fixed charges on the mobile ions has also been modeled by Manning's counter-ion condensation theory, but only for single salts [26,31]. Here, we generalize Manning's equations [31] for ion diffusivity impediment with mixed salts:

$$\frac{D_i^{\rm m}}{D_i^{\rm s}} = f_{{\rm u},i} \phi_{\rm w} \left(\frac{\phi_{\rm w}}{2 - \phi_{\rm w}}\right)^2 \left(1 - \frac{z_i^2}{3}A\right)$$
 (18)

where  $\phi_{\rm w}$  is water volume fraction and the term  $\left(\frac{\phi_{\rm w}}{2-\phi_{\rm w}}\right)^2$  accounts for the tortuosity effect. The parameter A is a function of  $\xi$  and  $|c_{\rm x}|$  and accounts for the electrostatic effect. When no counterion condensation occurs (i.e.,  $\xi < \xi_{\rm cr}$ ),

$$A = \sum_{m_1 = -\infty}^{+\infty} \sum_{m_2 = -\infty}^{+\infty} \left[ \frac{|c_{\mathbf{x}}|}{\pi \xi^{-1} |c_{\mathbf{x}}| (m_1^2 + m_2^2) + \sum_i (z_i^2 c_i^{\mathbf{m}})} \right]^2$$
 (19)

and when counter-ion condensation occurs (i.e.,  $\xi > \xi_{cr}$ ),

$$A = \sum_{m_1 = -\infty}^{+\infty} \sum_{m_2 = -\infty}^{+\infty} \left[ \frac{\xi_{\rm cr} |c_{\rm x}|}{\pi |c_{\rm x}| (m_1^2 + m_2^2) + \xi \sum_i (z_i^2 c_i^{\rm m} f_{{\rm u},i})} \right]^2$$
(20)

where  $m_1$  and  $m_2$  are two non-zero summation indices (i.e.,  $(m_1, m_2) \neq (0,0)$ ) that come from the lattice assumption in Manning's theory [31]. We note that Eqs. (18–20) can reduce to single salts scenario where the system contains only one counter-ion (see Appendix A3 for derivation). Thus, counter-ion mobility selectivity inside the IEM can be then expressed as:

$$S_{i/j}^{u} = \frac{z_{i}D_{i}^{s}}{z_{j}D_{j}^{s}} \frac{f_{u,i}}{f_{u,j}} \frac{\left(1 - \frac{z_{i}^{2}}{3}A\right)}{\left(1 - \frac{z_{j}^{2}}{3}A\right)}$$
(21)

Eq. (21) shows that the tortuosity effect cancels out in the mobility selectivity as both counter-ions experience the effect to the same extent.

# 2.4 Model evaluation

219

220

221

222

223

224

225

226

In a recent work, Chen et al. [16] experimentally measured the equilibrium partition of KCl/NaCl and CaCl<sub>2</sub>/NaCl into a CEM (CSE, Astom Co., Japan), and the partition of NaNO<sub>3</sub>/NaCl and Na<sub>2</sub>SO<sub>4</sub>/NaCl into an AEM (ASE, Astom Co., Japan) as a function of external total salt concentration. In those experiments, the concentrations of counter-ions and co-ions inside IEMs were measured. Here, we compare the three models, i.e., the standard Donnan model, the Donnan-affinity (D-A) model, and the Donnan-Manning (D-M) model, in their ability to fit the membrane-

phase ion concentrations. The model inputs, outputs and fitting parameters are summarized in Table 1 and the fitted parameters are summarized in Table S2 and Table S3. Membrane-phase ion concentrations,  $c_i^{\rm m}$ , and the Donnan potential across the interface,  $\Delta \varphi$ , can be determined by solving the ion partition equation (Eq. (4), or (8) or (10)) with the charge neutrality condition (Eq. (5)) simultaneously. In the D-M model, we use the  $\xi$  value (for each IEM) fitted by Chen et al. [16] from single salt partition experiments, as  $\xi$  has been validated to be an intrinsic property of IEMs. As the experimentally observed membrane phase co-ion concentration is roughly an order of magnitude lower than the counter-ion concentration, we used weighted least squares fitting (with a weight of 10 for co-ion concentration residuals) to avoid strong bias toward the influence of counter-ions:

$$\beta = \underset{\beta}{\operatorname{argmin}} \sum_{k} \sum_{i} \left( \omega_{i} \left( c_{i,k}^{\text{m,exp}} - c_{i,k}^{\text{m,mod}}(\beta) \right) \right)^{2}$$
(22)

where  $c_{i,k}^{\text{m,exp}}$  and  $c_{i,k}^{\text{m,mod}}$  are experimentally measured and model predicted membrane phase ion concentration of ion i for the  $k^{\text{th}}$  data point, respectively,  $\omega_i$  is the weight coefficient (equals 1 for counter-ions and 10 for co-ions),  $\beta$  is the fitting parameter, which is  $\mu_i^{\text{ex}}$  in the D-A model and  $\Delta\mu_{i/j}^{\text{con}}$  in the D-M model.

Table 1. Comparison of partition models with mixed salts

	Ideal Donnan model	D-A model	D-M model
Inputs	$c_i^s, c_x$	$c_i^{\rm S}, c_{\rm x}$	$c_i^{\mathrm{s}}, c_{\mathrm{x}}, \gamma_i^{\mathrm{s}}, \xi$
Outputs	$c_i^{\mathrm{m}}, \Delta \varphi$	$c_i^{ m m}, \Delta arphi$	$c_i^{\mathrm{m}}, \Delta \varphi, \gamma_i^{\mathrm{m}}, f_{\mathrm{u},i}$
Fitting parameters	None	$\mu_i^{\text{ex}}$ (Eq. (8))	$\Delta\mu_{i/j}^{\mathrm{con}}$ (Eq. (16))
Model structure	Simple	Simple	Relatively complex

We further compare the three models using additional experimental results in literature, including the partition of NaNO<sub>3</sub>/NaCl and Na<sub>2</sub>SO<sub>4</sub>/NaCl into AEMs as a function of external salt concentration ratio as reported by Zou et al. [17], and the partition of K<sub>2</sub>SO<sub>4</sub>/Na<sub>2</sub>SO<sub>4</sub> and

MgSO<sub>4</sub>/Na<sub>2</sub>SO<sub>4</sub> into CEMs as reported by Luo et al. [18]. The membrane properties and the  $\xi$  for each IEM (as reported by the authors) in these studies are summarized in Table S1. We note that the D-M model and the D-A model were applied to only fit counter-ion concentrations inside IEMs from these two studies, as both studies did not measure co-ion partition. Finally, the generalized Manning's mobility model is applied to predict the mobility selectivity of different ion pairs and compared with experimental results reported in the studies by Zou et al. [17] and by Luo et al. [18]. The experimental mobility selectivity was estimated using Eq. (2) with overall ion-ion selectivity measured from ED experiments and partition selectivity from sorption experiments.

254

255

256

257

258

259

260

261

262

263

264

265

266

267

268

269

270

271

272

273

274

246

247

248

249

250

251

252

253

#### 3. Results and Discussion

#### 3.1 Partition as a function of external total salt concentration

Counter-ion partition and selectivity Experimental equilibrium partition results of K<sup>+</sup>/Na<sup>+</sup> and Ca<sup>2+</sup>/Na<sup>+</sup> into CSE and NO<sub>3</sub>-/Cl<sup>-</sup> and SO<sub>4</sub><sup>2-</sup>/Cl<sup>-</sup> into ASE as a function of external total salt concentration were fitted with the D-M model, the D-A model and the ideal Donann model (Figure 1). The ideal Donnan model cannot differentiate counter-ions with the same valence as valence is the only ion specific property used in the model and thus it predicts same concentrations inside IEMs for a pair of monovalent counter-ions (Figure 1 A and C). In contrast, the D-M model and the D-A model can capture the competitive partition of counter-ions with the same valence via the difference in counter-ion condensation energy and ion-membrane affinity (Eqs. (9 and 17)), respectively. In the case of Ca<sup>2+</sup>/Na<sup>+</sup> into a CEM, the ideal Donnan model predicts the partition well, meaning the Donnan effect may dominate the partition. The D-M model shows good agreement, but the D-A model overestimates Na<sup>+</sup> partition and underestimates Ca<sup>2+</sup> partition (Figure 1B). The deviation of the D-A model may be because we fitted K<sup>+</sup>/Na<sup>+</sup> and Ca<sup>2+</sup>/Na<sup>+</sup> partition simultaneously and assumed the mutual counter-ion Na<sup>+</sup> and the mutual co-ion Cl<sup>-</sup> having the same affinity in both cases. In other words, we assumed ion-membrane affinity to be an intrinsic property for a given pair of ion and membrane but independent of the co-existence of other ions.

Both the D-M and D-A models partially capture the partition difference of NO<sub>3</sub>-/Cl<sup>-</sup> but fail to fit the increasing NO<sub>3</sub>- uptake when external salt concentration increases, especially at lower

concentration range (Figure 1C). The deviation indicates that both models may miss consideration of a concentration-dependent effect, e.g., concentration-dependent affinity or condensation energy. Finite ion volume may also induce a concentration dependence as ions are modeled as point charges in both the D-M and D-A models, though NO<sub>3</sub>- and Cl- have similar hydrated radius and NO<sub>3</sub>- has a larger bare radius (Table S4). Another concentration effect may come from IEM's swelling [16]. Water volume fraction and membrane charge density (per volume of absorbed solution) vary with swelling degree, but the effect has not been accounted for in either model. In the case of SO<sub>4</sub><sup>2-</sup>/Cl<sup>-</sup>, the AEM preferably sorbed Cl<sup>-</sup> over SO<sub>4</sub><sup>2-</sup>. Both the D-M and D-A models fit well while the ideal Donnan model predicts the opposite selectivity (Figure 1D). The ideal Donnan model always predicts a stronger partition of counter-ions with a higher valence over ions with a lower valence (Eq. (6)). The weaker partition of SO<sub>4</sub><sup>2-</sup> is explained by a higher condensation energy in the D-M model and a lower affinity in the D-A model, respectively (Table S2 and S3).

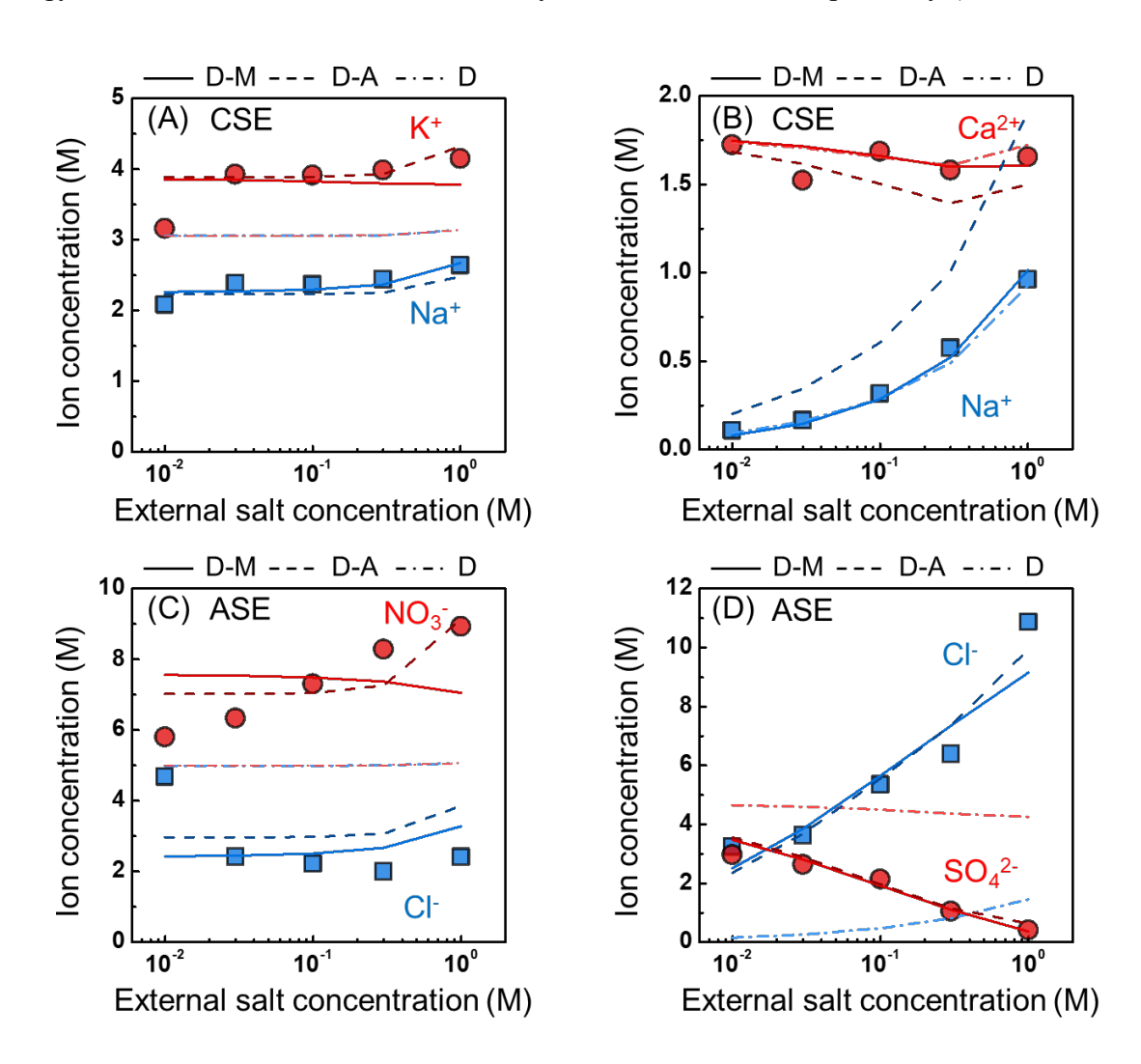


**Fig. 1** Partition of counter-ions into IEMs. (A) Na<sup>+</sup> and K<sup>+</sup> and (B) Na<sup>+</sup> and Ca<sup>2+</sup> concentrations inside the CSE (a type of CEM) as a function of external total salt concentration. External solution contains 1:1 molar ratio of NaCl/KCl or NaCl/MgCl<sub>2</sub>. (C) Cl<sup>-</sup> and NO<sub>3</sub><sup>-</sup> and (D) Cl<sup>-</sup> and SO<sub>4</sub><sup>2-</sup> concentrations inside the ASE (a type of AEM) as a function of external total salt concentration. External solution contains 1:1 molar ratio of NaCl/NaNO<sub>3</sub> or NaCl/Na<sub>2</sub>SO<sub>4</sub>. Symbols represent experimental data from reference [16]. Curves represent model fitting results from this study, including the Donnan model (curves D), Donnan Affinity model (curves D-A), and Donnan-Manning model (curves D-M).

The ideal Donnan model predicts no selectivity for the partition of monovalent ion pairs and the D-A model predicts a constant selectivity independent of ion concentration due to the assumption of constant affinity values. The D-M model predicts a slight decrease of monovalent ion partition selectivity for both cations (K<sup>+</sup>/Na<sup>+</sup>, Figure 2A) and anions (NO<sub>3</sub><sup>-</sup>/Cl<sup>-</sup>, Figure 2B) as external salt concentration increases. Both the D-A and D-M models fit K<sup>+</sup>/Na<sup>+</sup> selectivity reasonably well, but neither captures the slight increase in NO<sub>3</sub><sup>-</sup>/Cl<sup>-</sup> selectivity measured at a high external concentration (Figure 2B).

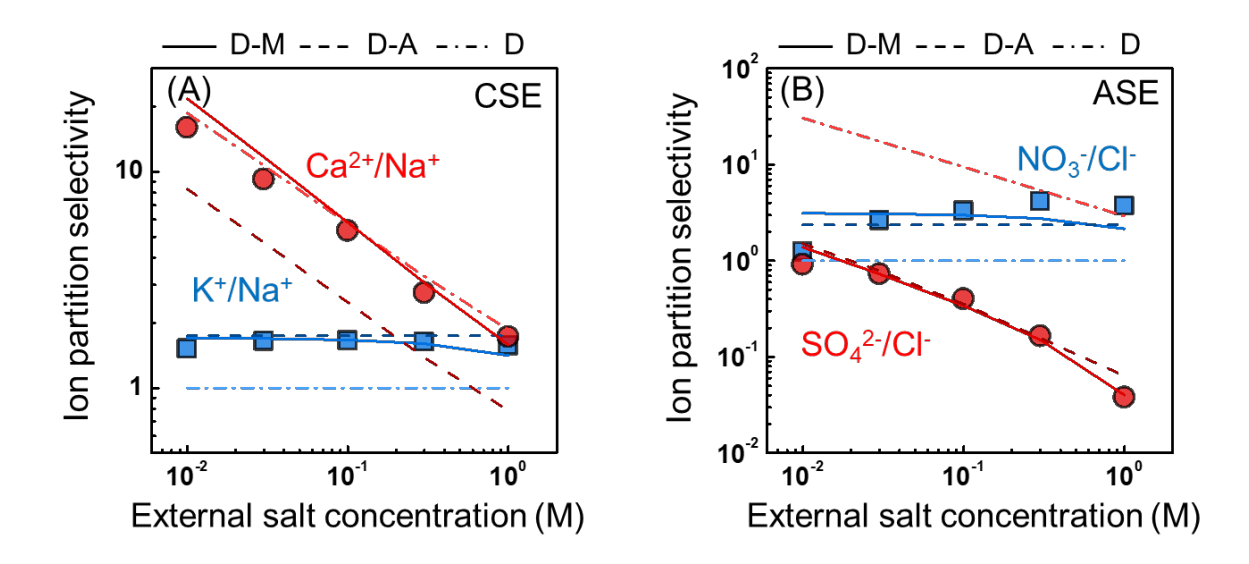


**Fig. 2** Ion-ion selectivity for counter-ion partition to IEMs. (A) K<sup>+</sup>/Na<sup>+</sup> and Ca<sup>2+</sup>/Na<sup>+</sup> partition selectivity of CSE. (B) NO<sub>3</sub>-/Cl<sup>-</sup> and SO<sub>4</sub><sup>2-</sup>/Cl<sup>-</sup> partition selectivity of ASE. External solution salt molar ratio is 1:1. Symbols represent experimental data from reference[16]. Lines represent model fitting results from this study.

Compared to the selectivity of monovalent counter-ion pairs which varies within one order of magnitude, divalent/monovalent ion selectivity decreases much more dramatically with increasing salt concentration for both cations (Figure 2A) and anions (Figure 2B), likely due to the charge screening effect. Such a dependence of selectivity on salt concentration is captured by all three models (Figure 2A). However, the ideal Donnan model fails to predict the preferable uptake of Cl<sup>-</sup> over SO<sub>4</sub><sup>2-</sup> (Figure 2B). The SO<sub>4</sub><sup>2-</sup>/ Cl<sup>-</sup> selectivity is lower than unity likely due to the lack of consideration of ion-membrane interaction. The D-A model underestimates Ca<sup>2+</sup>/Na<sup>+</sup> selectivity

by about half (Figure 2A) because of the overestimation of Na<sup>+</sup> partition (Figure 1B). Only the D-M model fits divalent/monovalent ion selectivity well in both CEM (Figure 2A) and AEM (Figure 2B).

Co-ion partition and selectivity Co-ion partition has received less attention as compared to counter-ion partition when evaluating ion-ion selectivity. Most studies reported in literature measured only the partition of counter-ions in the static sorption experiments [17,18,38,39]. Only a few reported both counter-ion and co-ion partitions [16,21,22]. Although co-ion concentration inside IEMs may be negligible as compared to the counter-ion concentration (which approaches membrane charge density if there is only one species of counter-ion) when the external solution is dilute, co-ion partition increases with increasing external salinity and becomes non-negligible when external concentration exceeds 0.1 M (Figure 3). Moreover, co-ion transport across IEMs is important as it reflects the non-ideality of IEMs and affects the current efficiency of ED processes, especially when back salt diffusion flux becomes non-negligible with a large salinity difference between the diluate and brine streams [28]. Thus, a partition model that can predict co-ion partition accurately is also essential to modeling an ED process.

From fitting results of co-ion (i.e., Cl<sup>-</sup> or Na<sup>+</sup>) partition into CSE and ASE with mixed salt solutions, the D-M model fits co-ion partition the best in all cases (Figure 3). Both the ideal Donnan model and the D-A model tend to underestimate the co-ion partition, with deviations within an order of magnitude. A better fitting of co-ion partition suggests that the D-M model likely better captures the physics of ion partition.

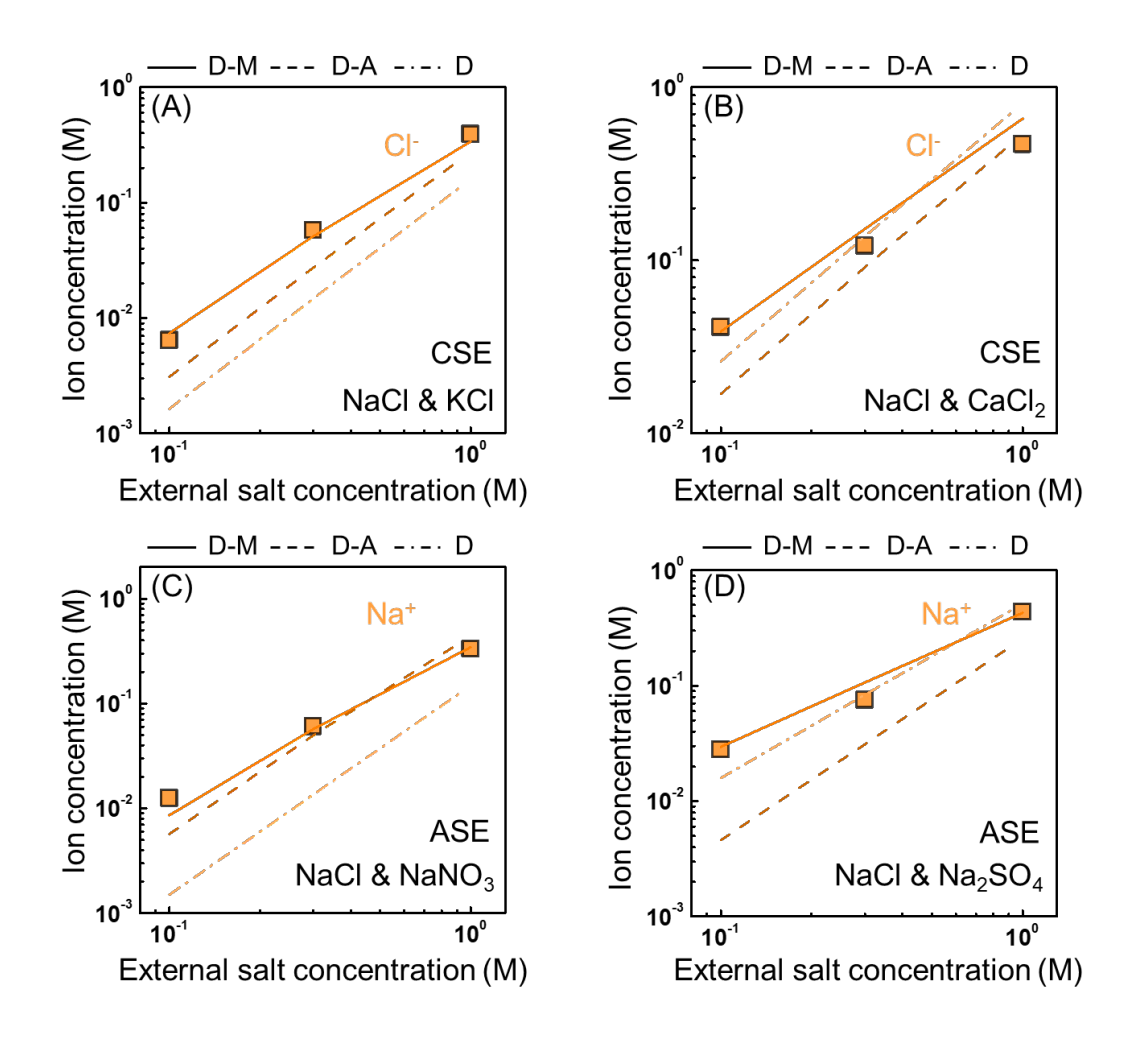
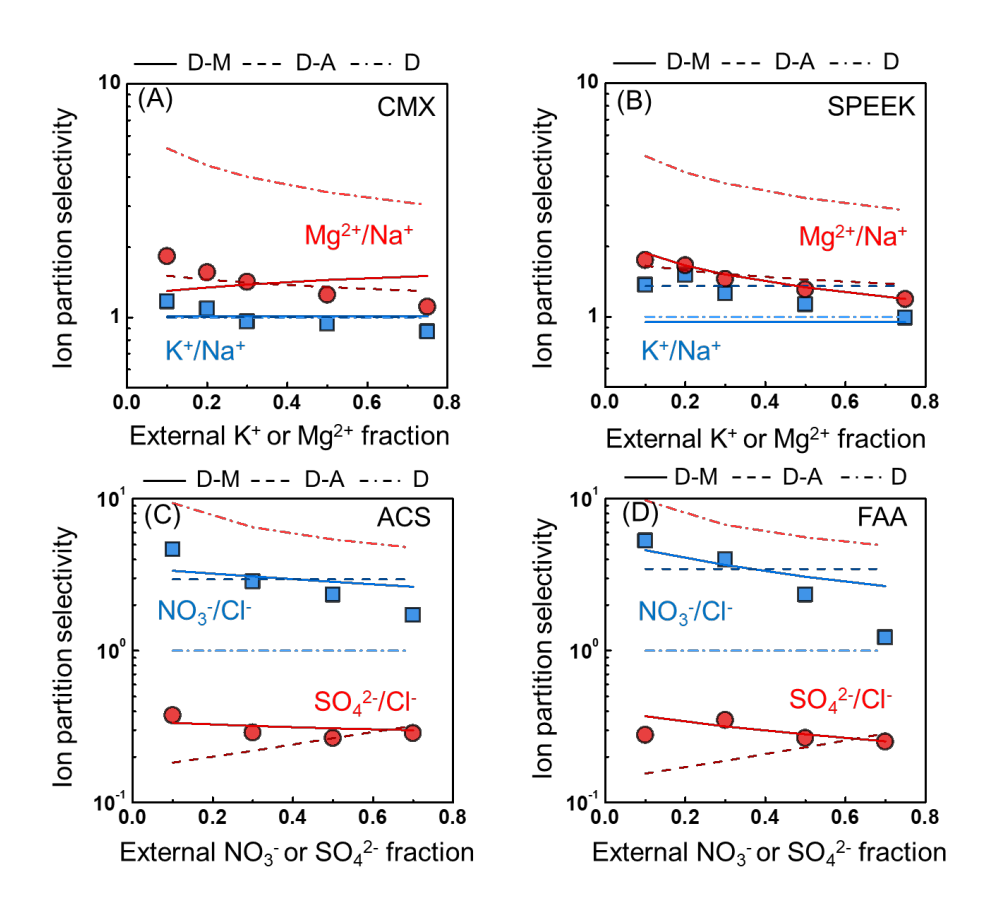


Fig. 3 Partition of co-ions into IEMs. Cl<sup>-</sup> concentration inside the CSE as a function of external total salt concentration when the external solution is a mixture of (A) NaCl/KCl and (B) NaCl/MgCl<sub>2</sub>. Na<sup>+</sup> concentration inside the ASE as a function of external total salt concentration when the external solution is a mixture of (C) NaCl/NaNO<sub>3</sub> and (D) NaCl/Na<sub>2</sub>SO<sub>4</sub>. External solution salt molar ratio is 1:1. Symbols represent experimental data from reference [16]. Lines represent model fitting results from this study.

#### 3.2 Ion partition as a function of external salt concentration ratio

To further compare their fitting capability and limitations, we evaluate the D-M model, the D-A model and the ideal Donann model in fitting experimental results of equilibrium partition of K<sup>+</sup>/Na<sup>+</sup> and Mg<sup>2+</sup>/Na<sup>+</sup> into two additional CEMs (CMX and SPEEK) and NO<sub>3</sub><sup>-</sup>/Cl<sup>-</sup> and SO<sub>4</sub><sup>2-</sup>/Cl<sup>-</sup> into two additional AEMs (ACS and FAA) (Figure S1-S2). For the partition of Mg<sup>2+</sup>/Na<sup>+</sup>, the ideal Donnan model overestimates the Mg<sup>2+</sup> uptake and thus predicts a high selectivity towards Mg<sup>2+</sup> (Figure 4A and B), contrasting its good prediction of Ca<sup>2+</sup>/Na<sup>+</sup> partition in CSE (Figure 2A). As Mg<sup>2+</sup> and Ca<sup>2+</sup> have similar properties (e.g., radius and hydration energy, Table S4), the deviation of the ideal Donnan model for the Mg<sup>2+</sup>/Na<sup>+</sup> case is likely caused by the difference of membrane

properties (e.g., CSE has a higher ion exchange capacity and water uptake than CMX and SPEEK, Table S1). But we also note that the co-ion species is different in the two cases (i.e., SO<sub>4</sub><sup>2-</sup> for Mg<sup>2+</sup>/Na<sup>+</sup> and Cl<sup>-</sup> for Ca<sup>2+</sup>/Na<sup>+</sup>), which may possibly affect the partition of counter-ions too.



**Fig. 4** Ion-ion partition selectivity of IEMs. K<sup>+</sup>/Na<sup>+</sup> and Mg<sup>2+</sup>/Na<sup>+</sup> partition selectivity of (A) CMX and (B) SPEEK. NO<sub>3</sub>-/Cl<sup>-</sup> and SO<sub>4</sub><sup>2-</sup>/Cl<sup>-</sup> partition selectivity of (C) ACS and (D) FAA. External co-ion concentration is 0.5 M. Symbols represent experimental data from references [17,18]. Lines represent model fitting results from this study.

The D-M and D-A models fit  $Mg^{2+}/Na^+$  partition in CMX and SPEEK reasonably well (Figure S1) because both models have extra membrane-dependent property information in additional to membrane charge density (as in the ideal Donnan model). Such information includes the Manning parameter and ion condensation energy in the D-M model, and the ion affinity in the D-A model (Table S2 and S3). We notice that the D-M model predicts a slight increase of  $Mg^{2+}/Na^+$  selectivity in CMX as external  $Mg^{2+}$  fraction increases (Figure 4A), which is opposite to the experimentally measured decrease of  $Mg^{2+}/Na^+$  selectivity from ~2 to ~1. However, the D-M model fits the decreasing trend well in SPEEK (Figure 4B).

For the partition of SO<sub>4</sub><sup>2</sup>-/Cl<sup>-</sup>, the D-M model fits the selectivity better than the D-A model (Figure 4 C and D), especially at low external SO<sub>4</sub><sup>2</sup>- fraction range, although both models fit ion concentrations inside the IEMs reasonably well (Figure S2). For the monovalent ion pairs, the ideal Donnan model predicts no selectivity and the D-A model can only fit a constant value as discussed before. The D-M model partially captures the decreasing trend of NO<sub>3</sub>-/Cl<sup>-</sup> selectivity when NO<sub>3</sub>- fraction in the external solution increases (Figure 4C and D).

#### 3.3 Impact of membrane properties on partition selectivity

In this section, we apply the generalized the D-M model to investigate the impact of IEM's properties on the partition selectivity of practically relevant ion pairs, e.g., Li<sup>+</sup> extraction from brine lakes where other cations exist in abundance. The major challenge of Li<sup>+</sup> extraction is that all cations have similar radius and properties (Table S4) and Li<sup>+</sup> usually has a much lower concentration [40]. One major purpose of membrane-based Li<sup>+</sup> separation is to remove Mg<sup>2+</sup> because MgCO<sub>3</sub> would otherwise co-exist in the Li<sub>2</sub>CO<sub>3</sub> precipitate formed in a later stage. Removal of other monovalent cations, like Na<sup>+</sup> and K<sup>+</sup>, is not as important (as they will not coprecipitate with Li<sub>2</sub>CO<sub>3</sub>) but the presence of these monovalent co-ions may affect the current efficiency of an ED process applied for selective Li<sup>+</sup> separation [12,14].

To get a qualitative understanding of the impact of membrane charge density, Manning parameter, and ion condensation energy difference on ion partition selectivity, we assume that these variables can be tuned independently (which is likely an oversimplification) as the physical relationships behind them are complicated or currently unclear. By increasing the charge density of the CEM, Li<sup>+</sup>/Mg<sup>2+</sup> selectivity decreases while Li<sup>+</sup>/Na<sup>+</sup> selectivity remains unchanged (Figure 5A). Increasing charge density would have a similar effect as reducing external salt concentration (Figure 2) that enhances the Donnan effect and promotes the uptake of counter-ions with a higher valence. Thus, a CEM with lower charge density benefits the counter-ion partition selectivity toward Li<sup>+</sup> though the effect is weak, although a lower charge density may reduce counter-ion/co-ion selectivity and thereby compromise charge efficiency.

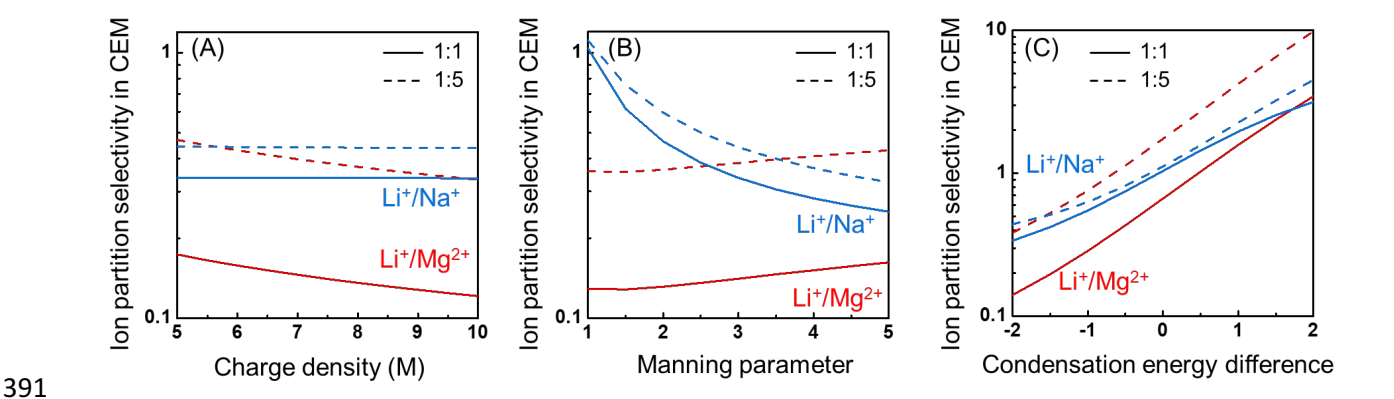


**Fig. 5** Li<sup>+</sup>/Mg<sup>2+</sup> and Li<sup>+</sup>/Na<sup>+</sup> partition selectivity in a hypothetical CEM as a function of (A) membrane charge density, (B) Manning parameter and (C) ion condensation energy difference under two concentration ratios. Charge density, Manning parameter and condensation energy difference were set as 7.5 M, 3, and -2, respectively, for the base case. External salt solution was assumed to be 50 mM LiCl and 50 mM (or 250 mM) MgCl<sub>2</sub> or NaCl for the 1:1 (or 1:5) case.

By increasing Manning parameter of the CEM, Li<sup>+</sup>/Mg<sup>2+</sup> selectivity increases while Li<sup>+</sup>/Na<sup>+</sup> selectivity decreases (Figure 5B). Manning parameter is a function of permittivity and distance between fixed charges and may be tuned by polymer hydrophobicity and the distribution of functional groups in the membrane matrix [20]. Assuming Manning parameter increases by reducing the permittivity within the polymer matrix, then counter-ions with lower hydration energy (Table S4) may preferably sorb to the membrane as they are easier to partially dehydrate. The permittivity related hydration effect has also been modeled by a hydration energy barrier via the Born model in previous studies of IEM and nanofiltration membrane [38,39,41,42], but the Born model tends to overestimate the energy barrier.

The variation of either charge density or Manning parameter has limited impact on increasing CEM selectivity towards Li<sup>+</sup> (Figure 5A and 5B). The most effective way is to increase ion condensation energy difference between Li<sup>+</sup> and other competitive cations, or in other words, increase membrane's affinity towards Li<sup>+</sup> (Figure 5C). Numerous studies have explored the use of coordination chemistry to enhance a CEM's selectivity towards a specific ion [43,44]. These approaches are in principle consistent with increasing membrane's affinity towards a specific ion of interest. Lastly, Li<sup>+</sup> partition selectivity is higher with a lower Li<sup>+</sup> concentration fraction in the external solution, which is consistent with previously discussed experimental trends for Mg<sup>2+</sup>/Na<sup>+</sup> and K<sup>+</sup>/Na<sup>+</sup> partition (Figure 4). We note that the D-M model is in principle only accurate for describing the behavior of homogeneous IEMs because it uses average membrane properties and

a mean field approximation [20]. However, in some cases it has been shown to be useful for describing the properties of heterogeneous membranes[33,35,45–47].

## 3.4 Mobility selectivity

Counter-ion mobility selectivity was back-calculated using Eq. (2) with overall ion-ion transport selectivity experimentally measured in the ED process and partition selectivity measured using sorption experiments with mixed salt solutions. We compare experimental results from Luo's and Zou's studies [17,18] with predictions of the generalized Manning's model for mixed salts (Eq. (21)). However, the mixed salt transport model based on the original Manning theory could not match experimental mobility selectivity well (Figure 6). One possible reason is the unclear impact of counter-ion condensation on mobility. In the original Manning's counter-ion condensation theory, condensed ions were assumed to be immobile [31]. However, Kamcev et al. measured counter-ion mobility inside IEMs with single salts and found that condensed ions may migrate twice as fast as the uncondensed ions under the electric field for Na<sup>+</sup> and Cl<sup>-</sup> in CEMs and AEMs, respectively [26]. Thus, the counter-ion diffusivity inside IEMs was suggested to be modeled as a weighted average of uncondensed and condensed parts:

$$D_i^{\rm m} = f_{{\rm u},i} D_{{\rm u},i}^{\rm m} + (1 - f_{{\rm u},i}) D_{{\rm c},i}^{\rm m}$$
(23)

where  $D_{\mathbf{u},i}^{\mathbf{m}}$  [m<sup>2</sup> s<sup>-1</sup>] is the diffusivity of uncondensed counter-ion and is modeled by Eq. (18),  $D_{\mathbf{c},i}^{\mathbf{m}}$ [m<sup>2</sup> s<sup>-1</sup>] is the diffusivity of condensed counter-ion. If we assume  $D_{\mathbf{c},i}^{\mathbf{m}} = \alpha D_{\mathbf{u},i}^{\mathbf{m}}$  and counter-ion mobility selectivity inside the IEM can be then expressed as:

$$S_{i/j}^{u} = \frac{z_{i}D_{i}^{s}}{z_{j}D_{j}^{s}} \frac{\left(\alpha + (1-\alpha)f_{u,i}\right)}{\left(\alpha + (1-\alpha)f_{u,j}\right)} \frac{\left(1 - \frac{z_{i}^{2}}{3}A\right)}{\left(1 - \frac{z_{j}^{2}}{3}A\right)}$$
(24)

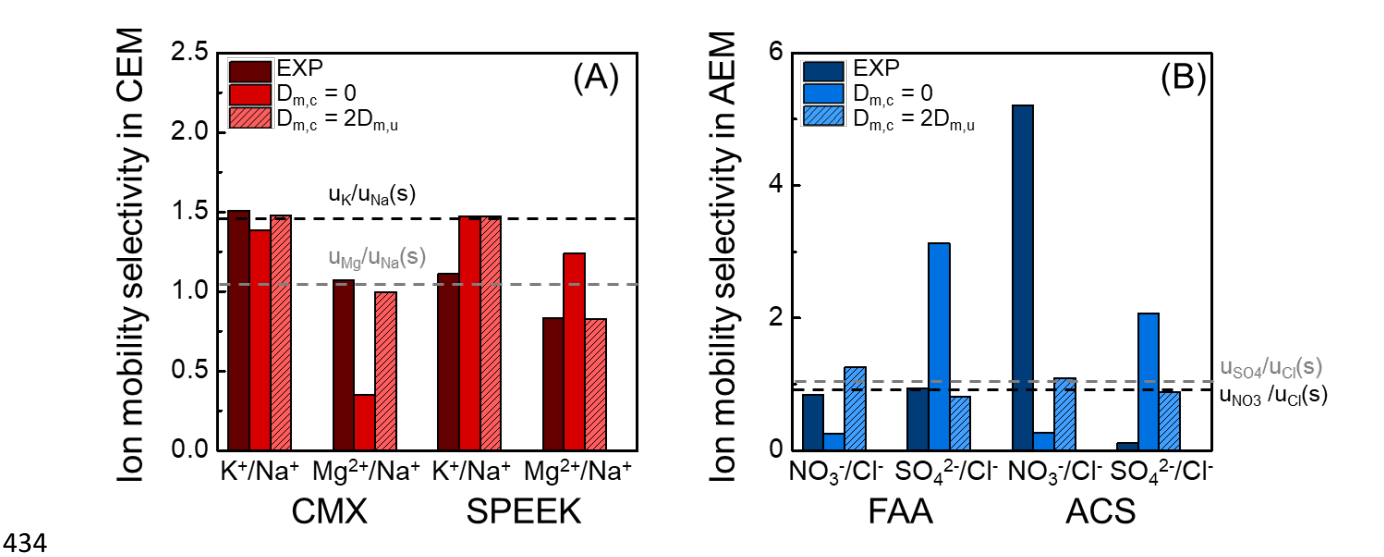


**Fig. 6** Ion mobility selectivity of IEMs. Experimental and model predicted (A) K<sup>+</sup>/Na<sup>+</sup> and Mg<sup>2+</sup>/Na<sup>+</sup> mobility selectivity of CMX and SPEEK. (B) NO<sub>3</sub>-/Cl<sup>-</sup> and SO<sub>4</sub><sup>2-</sup>/Cl<sup>-</sup> mobility selectivity of FAA and ACS. Dash lines indicate mobility selectivity in the external bulk salt solutions. Experimental data were from references [17,18].

After accounting for the mobility of condensed counter-ions (i.e., assume  $\alpha=2$  according to Kamcev's previous finding [26]), the predicted mobility selectivity is much closer to the experimental results than that predicted with the assumption of immobile condensed ions for both CEM (CMX and SPEEK) and for one AEM (FAA) (Figure 6). For the ACS membrane (an AEM), however, the Manning theory underestimates the mobility selectivity of  $NO_3^{-1}/Cl^{-1}$  and overestimate the mobility selectivity of  $SO_4^{2-1}/Cl^{-1}$  regardless of the assumption for condensed ion mobility (Figure 6). The deviations may arise from imperfection of the current theory or stem from the inaccuracy of the indirect determination of experimental mobility selectivity via Eq. (2) which assumes (a) electro-migration flux dominates counter-ion flux and (b) ion partition in the ED process is the same as that in the static sorption experiments. A more reliable experimental method for the direct measurement of individual ion diffusivity inside IEMs with mixed salts is needed to further validate the generalized Manning's model for mixed salts (predicted membrane phase ion diffusion coefficients are provided in Table S5). Moreover, it is worth to investigate whether ion partition is the same in the ED process and static sorption experiments, which can be more complex when the IEM is heterogeneous with a surface coating layer.

#### 4. Conclusions

We have extended the Manning's counter-ion condensation model for describing ion partition and ion mobility inside IEMs to mixed salts scenarios. The extended Donnan-Manning model was evaluated against experimental data from literature and compared with other two existing models, namely the ideal Donnan model, and the Donnan-Affinity model. In general, the Donnan-Manning model and the Donnan-Affinity model can provide reasonably accurate prediction of ion partition into IEMs in multiple scenarios, whereas the ideal Donnan model falls short in predicting any selectivity for ions with the same valence. We showed that the Donnan-Manning model can fit both counter-ion and co-ion partition well and outperform the Donnan-Affinity model in these regards. However, neither the Donnan-Manning model nor the Donnan-Affinity model can sufficiently capture the concentration dependences for counter-ion partition selectivity observed in all experiments. The generalized Manning's counter ion condensation theory has also been applied to predict counter-ion mobility selectivity. Applying the theory to experimental results suggests that the assumption of higher mobility of condensed ions than that of uncondensed ions seems to work better than the alternate assumption that condensed ions are immobile.

471

472

479

456

457

458

459

460

461

462

463

464

465

466

467

468

469

470

#### Acknowledgement

- 473 The authors acknowledge the support from the US National Science Foundation (#2017998),
- Water Research Foundation (Paul L. Busch Award to S.L.), and the National Alliance for Water
- Innovation (NAWI), funded by the U.S. Department of Energy, Office of Energy Efficiency and
- 476 Renewable Energy (EERE), Advanced Manufacturing Office, under Funding Opportunity
- 477 Announcement Number DE- FOA-0001905. The views expressed herein do not necessarily
- 478 represent the views of the U.S. Department of Energy or the United States Government.

## References

- 480 [1] R.M. DuChanois, C.J. Porter, C. Violet, R. Verduzco, M. Elimelech, Membrane Materials
- for Selective Ion Separations at the Water–Energy Nexus, Adv. Mater. 2101312 (2021) 1–
- 482 18. https://doi.org/10.1002/adma.202101312.
- 483 [2] S. Lin, M. Hatzell, R. Liu, G. Wells, X. Xie, Mining resources from water, Resour.

- 484 Conserv. Recycl. 175 (2021) 105853. https://doi.org/10.1016/j.resconrec.2021.105853.
- 485 [3] Y. Zhao, T. Tong, X. Wang, S. Lin, E.M. Reid, Y. Chen, Differentiating Solutes with
- 486 Precise Nanofiltration for Next Generation Environmental Separations: A Review,
- Environ. Sci. Technol. 55 (2021) 1359–1376. https://doi.org/10.1021/acs.est.0c04593.
- 488 [4] R.M. Duchanois, N.J. Cooper, B. Lee, S.K. Patel, L. Mazurowski, T.E. Graedel, M.
- 489 Elimelech, Prospects of Metal Recovery from Water, Nat. Water. 1 (2023) 1–20.
- 490 https://doi.org/10.1038/s44221-022-00006-z.
- 491 [5] H. Fan, Y. Huang, N.Y. Yip, Advancing ion-exchange membranes to ion-selective
- membranes: principles, status, and opportunities, Front. Environ. Sci. Eng. 17 (2023) 1–
- 493 27. https://doi.org/10.1007/s11783-023-1625-0.
- 494 [6] T. Luo, S. Abdu, M. Wessling, Selectivity of ion exchange membranes: A review, J.
- 495 Memb. Sci. 555 (2018) 429–454. https://doi.org/10.1016/j.memsci.2018.03.051.
- 496 [7] S.K. Patel, M. Qin, W.S. Walker, M. Elimelech, Energy Efficiency of Electro-Driven
- 497 Brackish Water Desalination: Electrodialysis Significantly Outperforms Membrane
- 498 Capacitive Deionization, Environ. Sci. Technol. 54 (2020) 3663–3677.
- 499 [8] S.K. Patel, P.M. Biesheuvel, M. Elimelech, Energy Consumption of Brackish Water
- Desalination: Identifying the Sweet Spots for Electrodialysis and Reverse Osmosis, ACS
- 501 ES&T Eng. (2021). https://doi.org/10.1021/acsestengg.0c00192.
- 502 [9] H. Strathmann, Ion-exchange membrane separation processes, Elsevier Science, 2004.
- 503 [10] C. Jiang, B. Chen, Z. Xu, X. Li, Y. Wang, T. Xu, Ion-"distillation" for isolating lithium
- from lake brine, AIChE J. (2022). https://doi.org/10.1002/aic.17710.
- 505 [11] T.M. Mubita, S. Porada, P.M. Biesheuvel, A. van der Wal, J.E. Dykstra, Strategies to
- increase ion selectivity in electrodialysis, Sep. Purif. Technol. 292 (2022) 120944.
- 507 https://doi.org/10.1016/j.seppur.2022.120944.
- 508 [12] J. Ying, M. Luo, Y. Jin, J. Yu, Selective separation of lithium from high Mg/Li ratio brine
- using single-stage and multi-stage selective electrodialysis processes, Desalination. 492
- 510 (2020) 114621. https://doi.org/10.1016/j.desal.2020.114621.

- 511 [13] Q.B. Chen, Z.Y. Ji, J. Liu, Y.Y. Zhao, S.Z. Wang, J.S. Yuan, Development of recovering
- lithium from brines by selective-electrodialysis: Effect of coexisting cations on the
- 513 migration of lithium, J. Memb. Sci. 548 (2018) 408–420.
- 514 https://doi.org/10.1016/j.memsci.2017.11.040.
- 515 [14] P.Y. Ji, Z.Y. Ji, Q.B. Chen, J. Liu, Y.Y. Zhao, S.Z. Wang, F. Li, J.S. Yuan, Effect of
- coexisting ions on recovering lithium from high Mg2+/Li+ ratio brines by selective-
- electrodialysis, Sep. Purif. Technol. 207 (2018) 1–11.
- 518 https://doi.org/10.1016/j.seppur.2018.06.012.
- 519 [15] H. Luo, W.A.S. Agata, G.M. Geise, Connecting the Ion Separation Factor to the Sorption
- and Diffusion Selectivity of Ion Exchange Membranes, Ind. Eng. Chem. Res. 59 (2020)
- 521 14189–14206. https://doi.org/10.1021/acs.iecr.0c02457.
- 522 [16] G.Q. Chen, K. Wei, A. Hassanvand, B.D. Freeman, S.E. Kentish, Single and binary ion
- sorption equilibria of monovalent and divalent ions in commercial ion exchange
- membranes, Water Res. 175 (2020) 115681. https://doi.org/10.1016/j.watres.2020.115681.
- 525 [17] Z. Zou, L. Wu, T. Luo, Z. Yan, X. Wang, Assessment of anion exchange membrane
- selectivity with ionic membrane conductivity, revised with Manning's theory or the
- 527 Kohlrausch's law, J. Memb. Sci. 635 (2021) 119496.
- 528 https://doi.org/10.1016/j.memsci.2021.119496.
- 529 [18] T. Luo, Y. Zhong, D. Xu, X. Wang, M. Wessling, Combining Manning's theory and the
- ionic conductivity experimental approach to characterize selectivity of cation exchange
- 531 membranes, J. Memb. Sci. 629 (2021) 119263.
- 532 https://doi.org/10.1016/j.memsci.2021.119263.
- 533 [19] S. Ozkul, J.J. van Daal, N.J.M. Kuipers, R.J.M. Bisselink, H. Bruning, J.E. Dykstra,
- H.H.M. Rijnaarts, Transport mechanisms in electrodialysis: The effect on selective ion
- transport in multi-ionic solutions, J. Memb. Sci. 665 (2023) 121114.
- 536 https://doi.org/10.1016/j.memsci.2022.121114.
- 537 [20] D. Kitto, J. Kamcev, Manning condensation in ion exchange membranes: A review on ion
- partitioning and diffusion models, J. Polym. Sci. (2022) 1–45.

- https://doi.org/10.1002/pol.20210810.
- 540 [21] J. Kamcev, D.R. Paul, B.D. Freeman, Ion activity coefficients in ion exchange polymers:
- Applicability of Manning's counterion condensation theory, Macromolecules. 48 (2015)
- 542 8011–8024. https://doi.org/10.1021/acs.macromol.5b01654.
- 543 [22] J. Kamcev, M. Galizia, F.M. Benedetti, E.S. Jang, D.R. Paul, B.D. Freeman, G.S.
- Manning, Partitioning of mobile ions between ion exchange polymers and aqueous salt
- solutions: Importance of counter-ion condensation, Phys. Chem. Chem. Phys. 18 (2016)
- 546 6021–6031. https://doi.org/10.1039/c5cp06747b.
- 547 [23] R.S. Kingsbury, O. Coronell, Modeling and validation of concentration dependence of ion
- exchange membrane permselectivity: Significance of convection and Manning's counter-
- ion condensation theory, J. Memb. Sci. 620 (2021) 118411.
- https://doi.org/10.1016/j.memsci.2020.118411.
- R. Wang, J. Zhang, C.Y. Tang, S. Lin, Understanding Selectivity in Solute-Solute
- Separation: Definitions, Measurements, and Comparability, Environ. Sci. Technol. 56
- 553 (2022) 2605–2616. https://doi.org/10.1021/acs.est.1c06176.
- 554 [25] T. Luo, F. Roghmans, M. Wessling, Ion mobility and partition determine the counter-ion
- selectivity of ion exchange membranes, J. Memb. Sci. 597 (2020) 117645.
- 556 https://doi.org/10.1016/j.memsci.2019.117645.
- 557 [26] J. Kamcev, D.R. Paul, G.S. Manning, B.D. Freeman, Ion Diffusion Coefficients in Ion
- Exchange Membranes: Significance of Counterion Condensation, Macromolecules. 51
- 559 (2018) 5519–5529. https://doi.org/10.1021/acs.macromol.8b00645.
- 560 [27] H. Fan, Y. Huang, I.H. Billinge, S.M. Bannon, G.M. Geise, N.Y. Yip, Counterion
- Mobility in Ion-Exchange Membranes: Spatial Effect and Valency-Dependent
- Electrostatic Interaction, ACS ES T Eng. 2 (2022) 1274–1286.
- 563 https://doi.org/10.1021/acsestengg.1c00457.
- 564 [28] H. Strathmann, Ion-exchange membrane separation processes, 1st ed., Elsevier Science,
- 565 2004.
- 566 [29] K.S. Pitzer, G. Mayorga, Thermodynamics of electrolytes. II. Activity and osmotic

- coefficients for strong electrolytes with one or both ions univalent, J. Phys. Chem. 77
- 568 (1973) 2300–2308. https://doi.org/10.1021/j100638a009.
- 569 [30] K.S. Pitzer, J.J. Kim, Thermodynamics of Electrolytes. IV. Activity and Osmotic
- 570 Coefficients for Mixed Electrolytes, J. Am. Chem. Soc. 96 (1974) 5701–5707.
- 571 https://doi.org/10.1021/ja00825a004.
- 572 [31] G.S. Manning, Limiting laws and counterion condensation in polyelectrolyte solutions II.
- 573 Self-diffusion of the small ions, J. Chem. Phys. 51 (1969) 934–938.
- 574 https://doi.org/10.1063/1.1672158.
- 575 [32] G.S. Manning, Limiting laws and counterion condensation in polyelectrolyte solutions. I.
- 576 Colligative properties, J. Chem. Phys. 51 (1969) 924–933.
- 577 https://doi.org/10.1021/j150611a011.
- 578 [33] J. Kamcev, M. Galizia, F.M. Benedetti, E.S. Jang, D.R. Paul, B.D. Freeman, G.S.
- Manning, Partitioning of mobile ions between ion exchange polymers and aqueous salt
- solutions: Importance of counter-ion condensation, Phys. Chem. Chem. Phys. 18 (2016)
- 581 6021–6031. https://doi.org/10.1039/c5cp06747b.
- 582 [34] J. Kamcey, D.R. Paul, G.S. Manning, B.D. Freeman, Predicting salt permeability
- coefficients in highly swollen, highly charged ion exchange membranes, ACS Appl.
- Mater. Interfaces. 9 (2017) 4044–4056. https://doi.org/10.1021/acsami.6b14902.
- 585 [35] R. Sujanani, L.E. Katz, D.R. Paul, B.D. Freeman, Aqueous ion partitioning in Nafion:
- Applicability of Manning's counter-ion condensation theory, J. Memb. Sci. 638 (2021)
- 587 119687. https://doi.org/10.1016/j.memsci.2021.119687.
- 588 [36] G.S. Manning, Limiting laws and counterion condensation in polyelectrolyte solutions 8.
- Mixtures of counterions, species selectivity, and valence selectivity, J. Phys. Chem. 88
- 590 (1984) 6654–6661. https://doi.org/10.1063/1.1672158.
- 591 [37] J.S. Mackie, P. Mears, The Diffusion of Electrolytes in a Cation-exchange Resin
- 592 Membrane I. Theoretical, Proc. R. Soc. A. 232 (1955) 498–509.
- 593 https://doi.org/10.1098/rspa.1955.0234.
- 594 [38] R. Tandon, P.N. Pintauro, Divalent/monovalent cation uptake selectivity in a Nafion

- cation-exchange membrane: Experimental and modeling studies, J. Memb. Sci. 136
- 596 (1997) 207–219. https://doi.org/10.1016/S0376-7388(97)00167-1.
- 597 [39] T. Malewitz, P.N. Pintauro, D. Rear, Multicomponent absorption of anions in commercial
- 598 anion-exchange membranes, J. Memb. Sci. 301 (2007) 171–179.
- 599 https://doi.org/10.1016/j.memsci.2007.06.014.
- 600 [40] S. Xu, J. Song, Q. Bi, Q. Chen, W. Zhang, Z. Qian, L. Zhang, S. Xu, N. Tang, T. He,
- Extraction of lithium from Chinese salt-lake brines by membranes: Design and practice, J.
- 602 Memb. Sci. 635 (2021).
- 603 [41] R. Wang, S. Lin, Pore model for nanofiltration: History, theoretical framework, key
- predictions, limitations, and prospects, J. Memb. Sci. 620 (2021) 118809.
- https://doi.org/10.1016/j.memsci.2020.118809.
- 606 [42] Y. Ji, H. Luo, G.M. Geise, Specific co-ion sorption and diffusion properties influence
- membrane permselectivity, J. Memb. Sci. 563 (2018) 492–504.
- 608 https://doi.org/10.1016/j.memsci.2018.06.010.
- 609 [43] Y. Dong, Y. Liu, H. Li, Q. Zhu, M. Luo, H. Zhang, B. Ye, Z. Yang, T. Xu, Crown ether-
- based Tröger's base membranes for efficient Li+/Mg2+ separation, J. Memb. Sci. 665
- 611 (2023) 121113. https://doi.org/10.1016/j.memsci.2022.121113.
- 612 [44] A. Iddya, P. Zarzycki, R. Kingsbury, C.M. Khor, S. Ma, J. Wang, I. Wheeldon, Z.J. Ren,
- E.M.V. Hoek, D. Jassby, A reverse-selective ion exchange membrane for the selective
- transport of phosphates via an outer-sphere complexation—diffusion pathway, Nat.
- 615 Nanotechnol. 17 (2022) 1222–1228. https://doi.org/10.1038/s41565-022-01209-x.
- 616 [45] J. Kamcey, D.R. Paul, B.D. Freeman, Equilibrium ion partitioning between aqueous salt
- solutions and inhomogeneous ion exchange membranes, Desalination. 446 (2018) 31–41.
- 618 https://doi.org/10.1016/j.desal.2018.08.018.
- 619 [46] E.S. Jang, J. Kamcev, K. Kobayashi, N. Yan, R. Sujanani, S.J. Talley, R.B. Moore, D.R.
- Paul, B.D. Freeman, Effect of Water Content on Sodium Chloride Sorption in Cross-
- Linked Cation Exchange Membranes, Macromolecules. 52 (2019) 2569–2579.
- 622 https://doi.org/10.1021/acs.macromol.8b02550.

[47] J. Kamcev, D.R. Paul, B.D. Freeman, Effect of fixed charge group concentration on equilibrium ion sorption in ion exchange membranes, J. Mater. Chem. A. 5 (2017) 4638–4650. https://doi.org/10.1039/c6ta07954g.

## 628 Appendix

629

#### A1. Derivation of the generalized Manning's model

Here, we follow Manning's original work to derive activity coefficients of mobile ions in polyelectrolyte solutions from the excess Helmholtz free energy ( $F^{ex}$ ) [32]:

$$\ln(\gamma_i^{\rm m}) = \frac{\partial (F^{\rm ex}/VRT)}{\partial c_i^{\rm m}} = \frac{\partial (-\xi|c_{\rm x}|\ln\kappa)}{\partial c_i^{\rm m}}$$
(S1)

- where  $\kappa$  is the Debye screening parameter. By applying the generalized form of the Debye screening parameter,  $\kappa^2 = \lambda_B \sum_i (z_i^2 c_i^m)$ , Eq. (S1) results in Eq. (11) in the main text.
- When counter-ion condensation occurs (i.e.,  $\xi > \xi_{cr}$ ), ion activity can be expressed in terms of either stoichiometric quantities or effective quantities (after condensed counter-ions screening part of fixed charge groups) [32]:

$$a_i^{\rm m} = \gamma_i^{\rm m} c_i^{\rm m} = \gamma_i^{\rm m,eff} c_i^{\rm m,eff}$$
 (S2)

- where the effective ion concentration,  $c_i^{m,eff}$ , refers to the uncondensed fraction of ion
- concentration,  $c_i^{\text{m,eff}} = f_{\text{u},i} c_i^{\text{m}}$ . The effective activity coefficient,  $\gamma_i^{\text{m,eff}}$ , is evaluated via Eq. (11)
- by substituting  $\xi$  and  $|c_x|$  by  $\xi_{cr}$  and the effective charge density  $\frac{\xi_{cr}}{\xi}|c_x|$ , respectively. The Debye
- screening parameter should also be evaluated using uncondensed fraction of ion concentrations.
- Thus,  $\gamma_i^{\rm m} = f_{{\rm u},i} \gamma_i^{\rm m,eff}$ , which then leads to Eqs. (13-14) in the main text.
- Manning also expressed diffusion coefficients of uncondensed ions in terms of the Fourier components of the electrostatic potential set up by the fixed polyions [31]:
  - $\frac{D_{u,i}^{m}}{D_{i}^{s}} = \left(1 \frac{z_{i}^{2}}{3} \sum_{q} |\varphi_{q}|^{2}\right)$  (S3)

where  $\sum_{\mathbf{q}} |\varphi_{\mathbf{q}}|^2$  is equivalent to the parameter *A* in Eqs. (18-20) in the main text. The Fourier

component can be expressed as [31]:

$$\varphi_{q} = 4\pi \xi a^{-2} (q^{2} + \kappa^{2})^{-1}$$
 (S4)

where  $q = 2\pi a^{-1}(m_1, m_2)$  represents the coordinate vectors with distribution periodicity as the polyions are considered in a lattice space. The periodic unit volume containing a single fixed

charge is  $a^2b$  (i.e.,  $|c_x| = 1/a^2b$ ). Applying the generalized form of the Debye screening parameter in Eq. (S4) results in Eq. (19) in the main text for uncondensed case. For condensed case,  $\xi$  and  $|c_x|$  in Eq. (19) are replaced by  $\xi_{cr}$  and the effective charge density  $\frac{\xi_{cr}}{\xi}|c_x|$ , respectively, which results in Eq. (20) in the main text.

652

653

654

655

656

657

## A2. Derivation of activity coefficient expressions for single salts

Here, we present the derivation of activity coefficient expressions for the single salt case when condensation occurs (i.e.,  $\xi > \xi_{cr}$ ) from the general expressions in the main text. We use subscripts g and c to represent counter-ion and co-ion, respectively, consistent with literature [20–22]. For a single salt, Eq. (13) becomes:

$$\ln(\gamma_{\rm c}^{\rm m}) = -\frac{\xi_{\rm cr}^2 |c_{\rm x}| z_{\rm c}^2}{2\xi \left(z_{\rm g}^2 c_{\rm g}^{\rm m} f_{\rm u,g} + z_{\rm c}^2 c_{\rm c}^{\rm m}\right)}$$
(S5)

As there is only one counter-ion in the single salt, Eq. (15) becomes:

$$|z_{\mathsf{g}}|c_{\mathsf{g}}^{\mathsf{m}}\left(1 - f_{\mathsf{u},\mathsf{g}}\right) = |c_{\mathsf{x}}|\left(1 - \frac{\xi_{\mathsf{cr}}}{\xi}\right) \tag{S6}$$

By substituting Eq. (S2) into Eq. (S1), and combined with the electro-neutrality condition inside the IEM (Eq. (5)), we get:

$$\ln(\gamma_{c}^{m}) = -\frac{\xi_{cr}^{2}|c_{x}|z_{c}^{2}}{2\xi\left(|z_{g}z_{c}|c_{c}^{m} + |z_{g}c_{x}|\frac{\xi_{cr}}{\xi} + z_{c}^{2}c_{c}^{m}\right)}$$
(S7)

By defining X as the ratio of the fixed charge density to the salt concentration inside the IEM, i.e.,

662  $X = |c_x|/c_s^m$ , where  $c_s^m = c_c^m/\nu_c$ , and  $\nu_c$  and  $\nu_g$  are dissociation constants of the single salt (e.g.,

663  $\nu_c = 2$  and  $\nu_g = 1$  for MgCl<sub>2</sub>), Eq. (S7) can be re-organized as:

$$\ln(\gamma_{c}^{m}) = -\frac{\xi_{cr}^{2} z_{c}^{2} X}{2\xi \left( |z_{g} z_{c}| \nu_{c} + |z_{g}| \frac{\xi_{cr}}{\xi} X + z_{c}^{2} \nu_{c} \right)}$$
(S8)

Recall  $\xi_{\rm cr}=1/|z_{\rm g}|$ , and apply the relation  $|z_{\rm c}|\nu_{\rm c}=|z_{\rm g}|\nu_{\rm g}$ , Eq. (S8) becomes:

$$\ln(\gamma_{\rm c}^{\rm m}) = -\frac{1}{2} * \frac{\left(\frac{z_{\rm c}}{z_{\rm g}}\right)^2 X}{X + \frac{\xi}{\xi_{\rm cr}} |z_{\rm c}| \left(\nu_{\rm c} + \nu_{\rm g}\right)}$$
 (S9)

From Eq. (S6), the uncondensed fraction of counter-ion,  $f_{u,g}$ , can be expressed as:

$$f_{\text{u,g}} = 1 - \frac{|c_{\text{x}}| \left(1 - \frac{\xi_{\text{cr}}}{\xi}\right)}{|z_{\text{g}}| c_{\text{g}}^{\text{m}}}$$
 (S10)

which can be further transformed with the electro-neutrality condition and the introduction of X to:

$$f_{u,g} = \frac{|z_c|c_c^m + \frac{\xi_{cr}}{\xi}|c_x|}{|z_c|c_c^m + |c_x|} = \frac{|z_c|\nu_c + \frac{\xi_{cr}}{\xi}X}{|z_c|\nu_c + X} = \frac{|z_g|\nu_g + \frac{\xi_{cr}}{\xi}X}{|z_g|\nu_g + X}$$
(S11)

We note that Eqs. (S7 and S11) have the same form as literature studies [20]. The same derivations can be done for single salts when no condensation occurs (i.e.,  $\xi < \xi_{cr}$ ).

# A3. Derivation of diffusivity expressions for single salts

670

671

Here, we present the derivation of diffusion coefficient expressions for the single salt case when condensation occurs (i.e.,  $\xi > \xi_{cr}$ ) from the general expressions in the main text. For a single salt, the function A in Eq. (20) becomes:

$$A = \sum_{m_1 = -\infty}^{+\infty} \sum_{m_2 = -\infty}^{+\infty} \left[ \frac{\xi_{\rm cr} |c_{\rm x}|}{\pi |c_{\rm x}| (m_1^2 + m_2^2) + \xi (z_{\rm g}^2 c_{\rm g}^{\rm m} f_{\rm u,g} + z_{\rm c}^2 c_{\rm c}^{\rm m})} \right]^2$$
 (S12)

Following the same derivation procedure in Appendix A2, A becomes:

$$A = \sum_{m_1 = -\infty}^{+\infty} \sum_{m_2 = -\infty}^{+\infty} \left[ \frac{\xi_{\rm cr} |c_{\rm x}|}{\pi |c_{\rm x}| (m_1^2 + m_2^2) + \xi \left( |z_{\rm g} z_{\rm c}| c_{\rm c}^{\rm m} + |z_{\rm g} c_{\rm x}| \frac{\xi_{\rm cr}}{\xi} + z_{\rm c}^2 c_{\rm c}^{\rm m} \right)} \right]^2$$
 (S13)

Then, we recall  $\xi_{cr} = 1/|z_g|$ , introduce X and apply the relation  $|z_c|\nu_c = |z_g|\nu_g$ , Eq. (S13) becomes:

$$A = \sum_{m_1 = -\infty}^{+\infty} \sum_{m_2 = -\infty}^{+\infty} \frac{1}{z_g^2} \left[ \pi(m_1^2 + m_2^2) + 1 + \frac{\xi |z_c| (\nu_c + \nu_g)}{\xi_{cr} X} \right]^{-2}$$
 (S14)

We note that Eq. (S14) has the same form as literature studies [20], and the same derivations can be done for single salts when no condensation occurs (i.e.,  $\xi < \xi_{cr}$ ).

680

681

Table S1. IEM properties

			Ion exchange				
Type	Membrane	Manufacturer	capacity	Water	Manning	Ref.	
	Wiemorane	ivianata ctarer	(mmol per g	uptake (%)	parameter	TCT.	
			dry membrane)				
	CSE	Astom Co.,	2.07	30~37	2.8	[16]	
	CSL	Japan	2.07	30'-37	2.0	[10]	
CEMs	CMX	Astom Co.,	1.66	19~22	5.2	[18]	
		Japan	1.00	17 22	3.2	[10]	
	SPEEK	Lab-made	1.62	18~25	0.74	[18]	
	ASE	Astom Co.,	2.36	19~26	5.4	[16]	
	ASE	Japan	2.50	19.320	J. <b>T</b>	լոսյ	
	ACS Japan FuMa-To	Astom Co.,	2.02	21~25	5.8	[17]	
AEMs		Japan	2.02	21,323	J.0		
		FuMa-Tech					
		GmbH,	1.42	15~16	3.6	[17]	
		German					

682

**Table S2**. Fitted condensation energy difference  $(\Delta \mu_{i/j}^{\text{con}}/RT)$  in Donnan-Manning model

CEMs	K <sup>+</sup> vs Na <sup>+</sup>	Ca <sup>2+</sup> (Mg <sup>2+</sup> ) vs Na <sup>+</sup>	AEMs	NO <sub>3</sub> -vs Cl-	SO <sub>4</sub> <sup>2</sup> - vs Cl <sup>-</sup>
CSE	-0.86	-2.2	ASE	-1.49	1.28
CMX	-0.08	-1.79	ACS	-1.62	0.21
SPEEK	NA*	0.13	FAA	-2.15	0.82

**Table S3**. Fitted ion affinity  $(\mu_i^{\text{ex}}/RT)$  in Donnan-Affinity model

CEMs	K <sup>+</sup>	Na <sup>+</sup>	Ca <sup>2+</sup> (Mg <sup>2+</sup> )	Cl <sup>-</sup> (SO <sub>4</sub> <sup>2-</sup> )	AEMs	NO <sub>3</sub> -	Cl-	SO <sub>4</sub> <sup>2-</sup>	Na <sup>+</sup>
CSE	1.78	1.23	0.87	-0.92	ASE	4.00	3.15	0.54	-1.92
CMX	-2.37	-2.38	-6.32	0	ACS	-7.92	-9.01	-22.63	0
SPEEK	-2.18	-2.49	-6.31	0	FAA	-7.80	-9.04	-22.93	0

**Table S4**. Ion properties [54,55]

Ions	Bare radius (nm)	Hydrated radius (nm)	Enthalpy of hydration (kJ mol <sup>-1</sup> )	Diffusivity in water (10 <sup>-9</sup> m <sup>2</sup> s <sup>-1</sup> )
$K^+$	0.133	0.331	-322	1.95
$Na^+$	0.095	0.358	-409	1.33
$\mathrm{Li}^+$	0.06	0.382	-519	1.03
$\mathrm{Ca}^{2^+}$	0.099	0.412	-1577	0.92
${ m Mg^{2+}}$	0.065	0.428	-1921	0.707
$NO_3^-$	0.264	0.335	-314	1.70
Cl-	0.181	0.332	-381	2.03
SO <sub>4</sub> <sup>2</sup> -	0.29	0.379	-1059	1.06

**Table S5**. Predicted membrane phase ion diffusion coefficients (×10<sup>-11</sup> m<sup>2</sup> s<sup>-1</sup>)

CEMs	$K^+/Na^+$ $K^+$ $Na^+$		Mg <sup>2+</sup> /Na <sup>+</sup>		A EN C	NO <sub>3</sub> -/Cl-		SO <sub>4</sub> <sup>2-</sup> /Cl <sup>-</sup>	
CMX	6.76	4.58	2.81	5.71	ACS	4.99	4.55	3.08	6.94
CMX SPEEK	5.32	3.63	2.00	4.84	FAA	2.12	1.69	1.20	2.93

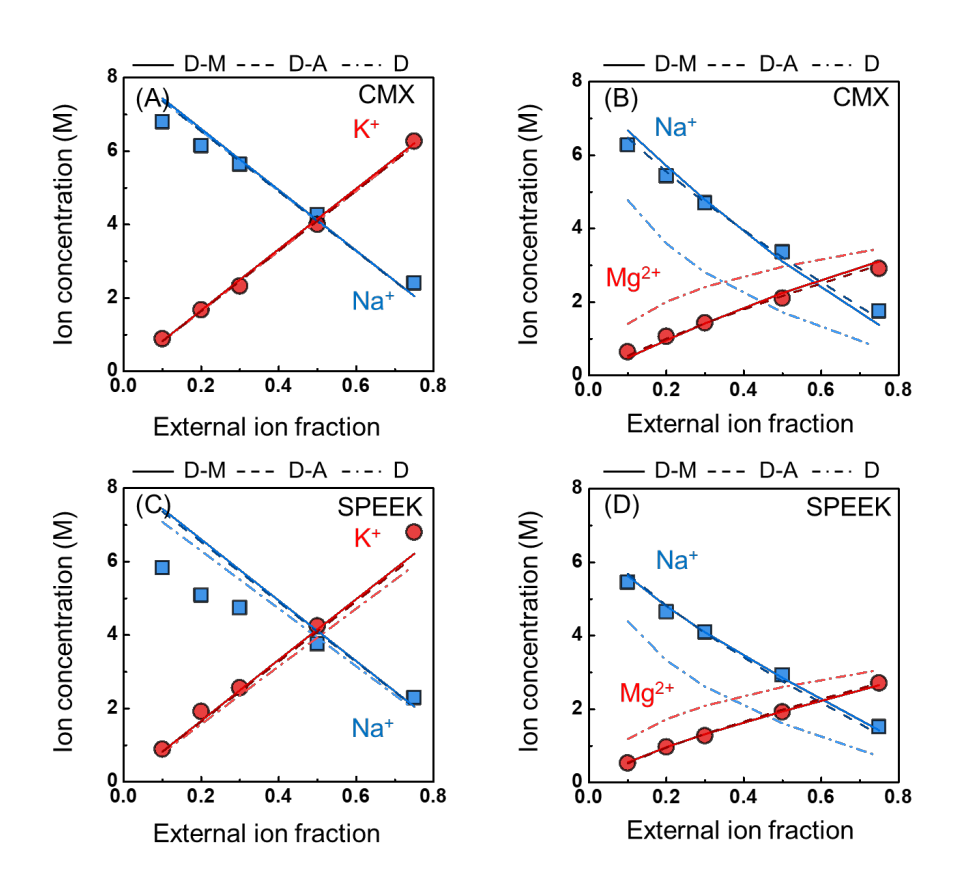


**Fig. S1** Partition of counter-ions into CEMs. (A) Na $^+$  and K $^+$  and (B) Na $^+$  and Mg $^{2+}$  concentrations inside the CMX as a function of external K $^+$  and Mg $^{2+}$  fraction. (C) Na $^+$  and K $^+$  and (D) Na $^+$  and Mg $^{2+}$  concentrations inside the SPEEK as a function of external K $^+$  and Ca $^{2+}$  fraction. External co-ion concentration is 0.5 M. Symbols represent experimental data from references [17,18]. Lines represent model fitting results from this study.

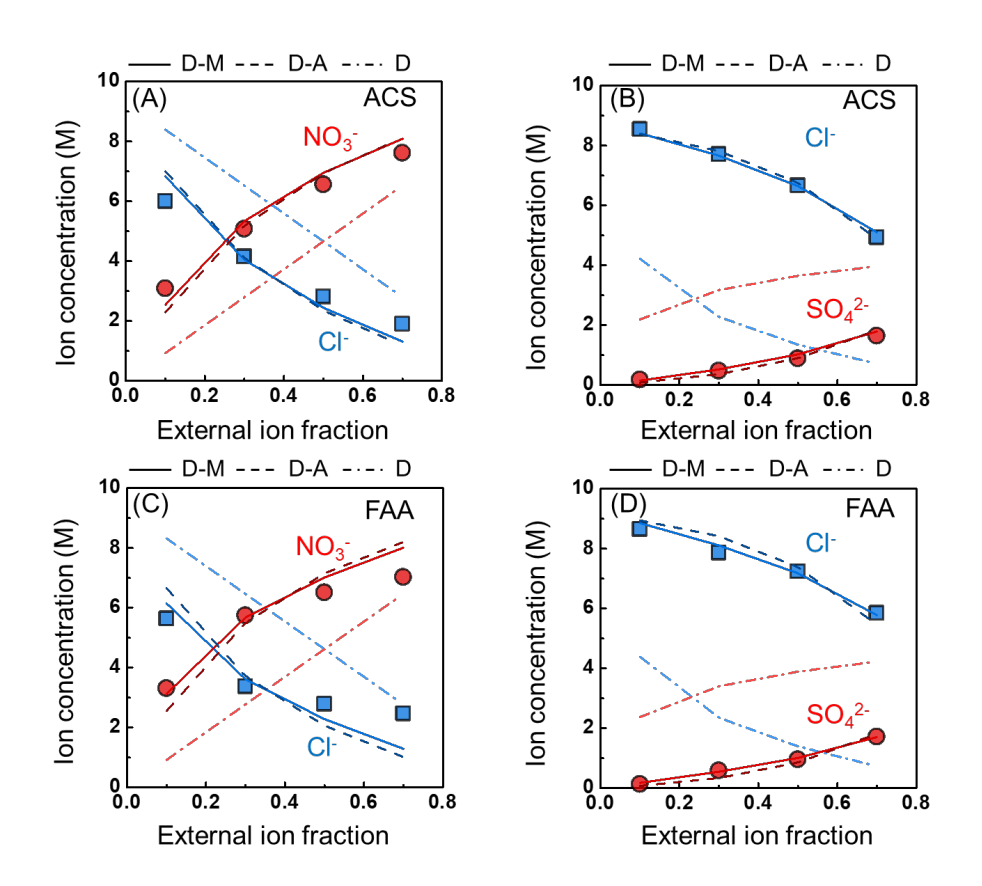


**Fig. S2** Partition of counter-ions into AEMs. (A) Cl<sup>-</sup> and NO<sub>3</sub><sup>-</sup> and (B) Cl<sup>-</sup> and SO<sub>4</sub><sup>2-</sup> concentrations inside the ACS as a function of external NO<sub>3</sub><sup>-</sup> and SO<sub>4</sub><sup>2-</sup> fraction. (C) Cl<sup>-</sup> and NO<sub>3</sub><sup>-</sup> and (D) Cl<sup>-</sup> and SO<sub>4</sub><sup>2-</sup> concentrations inside the FAA as a function of external NO<sub>3</sub><sup>-</sup> and SO<sub>4</sub><sup>2-</sup> fraction. External co-ion concentration is 0.5 M. Symbols represent experimental data from references [17,18]. Lines represent model fitting results from this study.